

# Structural Basis for Binding and Selectivity of Antimalarial and Anticancer Ethylenediamine Inhibitors to Protein Farnesyltransferase

Michael A. Hast,<sup>1</sup> Steven Fletcher,<sup>2</sup> Christopher G. Cummings,<sup>2</sup> Erin E. Pusateri,<sup>2</sup> Michelle A. Blaskovich,<sup>3</sup> Kasey Rivas,<sup>4</sup> Michael H. Gelb,<sup>5</sup> Wesley C. Van Voorhis,<sup>4</sup> Said M. Sebti,<sup>3</sup> Andrew D. Hamilton,<sup>2,6</sup> and Lorena S. Beese<sup>1,\*</sup>

<sup>1</sup>Department of Biochemistry, Duke University Medical Center, Box 3711, Durham, NC 27710, USA

<sup>2</sup>Department of Chemistry, Yale University, New Haven, CT 06511, USA

<sup>3</sup>Department of Drug Discovery, Moffitt Cancer Center and Research Institute, and Department of Oncologic Sciences, University of South Florida College of Medicine, Tampa, FL 33612, USA

<sup>4</sup>Department of Medicine

<sup>5</sup>Department of Chemistry

University of Washington, Seattle, WA 98195, USA

<sup>6</sup>Correspondence concerning inhibitor design and synthesis should be addressed to [andrew.hamilton@yale.edu](mailto:andrew.hamilton@yale.edu).

\*Correspondence: [lsb@biochem.duke.edu](mailto:lsb@biochem.duke.edu)

DOI 10.1016/j.chembiol.2009.01.014

## SUMMARY

Protein farnesyltransferase (FTase) catalyzes an essential posttranslational lipid modification of more than 60 proteins involved in intracellular signal transduction networks. FTase inhibitors have emerged as a significant target for development of anticancer therapeutics and, more recently, for the treatment of parasitic diseases caused by protozoan pathogens, including malaria (*Plasmodium falciparum*). We present the X-ray crystallographic structures of complexes of mammalian FTase with five inhibitors based on an ethylenediamine scaffold, two of which exhibit over 1000-fold selective inhibition of *P. falciparum* FTase. These structures reveal the dominant determinants in both the inhibitor and enzyme that control binding and selectivity. Comparison to a homology model constructed for the *P. falciparum* FTase suggests opportunities for further improving selectivity of a new generation of antimalarial inhibitors.

## INTRODUCTION

Development of protein farnesyltransferase (FTase) inhibitors (FTIs) for treatment of cancer has been a major focus for cancer chemotherapeutics research since the early 1990s (Basso et al., 2006). Oncogenic mutant forms of human Ras superfamily proteins are associated with 30% of all human cancers (Casey and Seabra, 1996a; Konstantinopoulos et al., 2007; Lane and Beese, 2006); the transforming ability of these mutants is dependent upon farnesylation (Casey and Seabra, 1996a). Two FTIs, Lonafarnib (Schering) and Tipifarnib (Johnson & Johnson) have advanced to late-stage clinical trials (Basso et al., 2006) for the treatment of certain cancers. More recently, FTase has emerged as a target for development of inhibitors to treat parasitic diseases caused by protozoan pathogens, including malaria

(*Plasmodium falciparum*), and African sleeping sickness (*Trypanosoma brucei*) (Eastman et al., 2006).

FTase catalyzes the transfer of a 15-carbon isoprenoid lipid moiety to the C terminus of more than 60 signal transduction proteins in the eukaryotic cell, including members of the Rho and Ras superfamily of G proteins (Casey and Seabra, 1996b; Reid et al., 2004b). Substrate proteins are modified at a carboxy-terminal peptide with a Ca<sub>1</sub>a<sub>2</sub>X motif, which consists of a cysteine (the  $\gamma$  sulfur is lipid modified), two generally aliphatic residues (a<sub>1</sub>a<sub>2</sub>), and a variable C-terminal (X) residue (Casey and Seabra, 1996b).

Crystal structures of catalytic reaction intermediates along the reaction cycle for mammalian FTase have been elucidated (Long et al., 2002; Taylor et al., 2003) and binding sites for substrates and products have been located (Long et al., 1998, 2000) (Figure 1). Kinetic analysis of the mechanism reveals that substrate binding is ordered (Dolence et al., 1995; Hightower et al., 1998; Tschantz et al., 1997; Zhang and Casey, 1996). The lipid complex forms first and the Ca<sub>1</sub>a<sub>2</sub>X tetrapeptide second. Binding of the lipid substrate FPP of the next turn of the reaction cycle is required to displace the isoprenoid moiety of the product from its original binding site into an “exit groove.” (Long et al., 2002; Taylor et al., 2003; Tschantz et al., 1997). The new Ca<sub>1</sub>a<sub>2</sub>X substrate binds after the product dissociates from the active site to continue the new cycle. Kinetic studies reveal that product release is the rate-limiting step in the reaction (Furfine et al., 1995; Huang et al., 2000; Pickett et al., 2003), an observation supported by the crystal structures of the displaced prenylated product complexes in FTase and the related protein geranylgeranyltransferase-I (GGTase-I) (Furfine et al., 1995; Long et al., 2002; Taylor et al., 2003).

A series of FTase inhibitors based on the ethylenediamine scaffold has been described recently (Glenn et al., 2006; Glenn et al., 2005). Here we also report the synthesis and properties of three new inhibitors in this series (Figures 2 and 3). The series is constructed out of relatively simple, flexible structures and can be prepared by straightforward chemical syntheses (Glenn et al., 2005, 2006). Members of this series are potent inhibitors of mammalian FTase (Glenn et al., 2006) and Table 1) and therefore

may provide new leads in cancer chemotherapeutic development. Several compounds also exhibit nanomolar  $IC_{50}$ s for the *P. falciparum* enzyme and are over 1000-fold selective for *P. falciparum* FTase over the human enzyme (Table 1) (Glenn et al., 2006).

Here we present the crystal structures of five members of the ethylenediamine-scaffold inhibitor series bound to mammalian FTase. These structures reveal two distinct binding modes for the inhibitors, which are different than originally predicted by molecular modeling (Glenn et al., 2005, 2006), but consistent with the observed structure-activity relationships. Of particular interest is a novel binding mode in which the inhibitor occupies parts of both the isoprenoid and protein substrate binding sites. This bisubstrate binding mode has not been observed previously and provides an opportunity to exploit the isoprenoid binding pocket for inhibitor design. All members of the series coordinate the catalytic  $Zn^{2+}$  via their *N*-methylimidazole group, contact the  $a_2$  residue binding site, and share a common moiety oriented toward the product exit groove. The structures presented provide a framework for refinement of inhibitor design to improve affinity for mammalian and parasite FTases. Of note, these inhibitors bind to two of the most cross-species, structurally divergent areas of the FTase active site. We propose that the observed selectivity of the ethylenediamine-scaffold inhibitor series for *P. falciparum* FTase is a consequence of inhibitor moieties contacting residues in these divergent regions.

## RESULTS

### Inhibitors

The ethylenediamine-scaffold-based FTIs (**2**, **4**, **5**, **7**, and **10**) studied in this work are illustrated in Figure 1B, and the  $IC_{50}$  values for human and *P. falciparum* FTase are given in Table 1.

### FTI Binding Does Not Induce Conformational Changes in FTase

The overall structure of the mammalian FTase heterodimer and the positions of the substrate (FPP and peptide) and product binding sites are shown in Figure 1. The  $\beta$  subunit (Figure 1A, blue) contains most of the substrate-binding residues and is partially enveloped by the crescent shaped  $\alpha$  subunit (Figure 1A, red). The central cavity of the  $\beta$  subunit accommodates the substrates bound in extended conformations side-by-side, with extensive contact between the binding sites (Long et al., 2000, 2002). The  $Ca_1a_2X$  substrate coordinates the catalytic  $Zn^{2+}$  via its cysteine SH group at the top of the cavity (Long et al., 2000). The product exit groove is a shallow hydrophobic binding site located adjacent to the  $Ca_1a_2X$  binding site, opposite the FPP binding site in the  $\beta$  subunit (Long et al., 2002).

The active site of FTase does not undergo significant conformational changes upon substrate binding or product release (Bell et al., 2002; Long et al., 2002; Reid and Beese, 2004; Reid et al., 2004a, 2004b). Binding of the ligands (inhibitors and isoprenoid diphosphate) observed here also does not induce significant structural changes in the active site. The all-atom rmsd values for the structures compared with the molecular replacement search models are within the experimental error of the coordinates ( $\sim 0.2\text{\AA}$ ). Inhibitors **2**, **4**, **7**, and **10** all occupy the portion of the active site normally occupied by protein substrate

and form a ternary complex with FPP (Figure 2). By contrast, **5** binds across both the peptide and isoprenoid binding sites, blocking the binding of both substrates (Figure 4). FPP was included with **5** during introduction of inhibitor into FTase crystals (see Experimental Procedures); however, only the inhibitor is observed in the active site. All inhibitors share two common substituents oriented identically in the active site: an *N*-methylimidazole moiety, which coordinates the catalytic  $Zn^{2+}$  ion in the active site; and a *para*-benzonitrile, which is directed toward the exit groove (Figures 2 and 5C). The identity of the other two substituents of the ethylenediamine scaffold appears to direct the binding mode.

### Ternary Complexes with **2**, **4**, and **7**

As shown in Figures 1B and 3, **2** and **4** differ by only a single substituent: the benzyl moiety of **2** is exchanged for an *N*-Boc-piperidin-4-ylmethyl in **4**. The binding mode of these two inhibitors is similar (Figures 2A, 2E, and 2F). As described above, the *para*-benzonitrile substituent is oriented toward the product exit groove and is partially stabilized by a stacking interaction with Y361 $\beta$ . The binding pocket also consists of residues D359 $\beta$ , F360 $\beta$ , Y93 $\beta$ , L96 $\beta$ , and W106 $\beta$ . Both **2** and **4** possess two *N*-methylimidazole moieties: one coordinates the catalytic  $Zn^{2+}$  (Figures 2A, 2E, and 2F); the second (at the sulfonamide position) is sandwiched between the first *N*-methylimidazole and the first isoprene of FPP. There is a single polar contact made between the imine nitrogen of the sulfonamide position *N*-methylimidazole and the side chain hydroxyl of Y361 $\beta$ .

The binding of **7** is similar to that of **2** (Figures 2D and 2F). The two variable substituents,  $R^1$  and the  $R^2$  sulfonyl group, bind in opposite orientations relative to **2**, with the sulfonamide position now directed toward the  $a_2$  residue binding site. However, the positions of the aromatic rings of **7** are similar to the rings at the  $R^1$  and  $R^2$  positions of **2**, with the phenyl ring stacking next to the  $Zn^{2+}$ -coordinating *N*-methylimidazole, and the *o*-methylphenyl group of **7** stabilized in a similar manner to the  $R^1$  phenyl substituent of **2**.

The  $R^1$  substituents of both **2** and **4** are directed toward the binding pocket for the  $Ca_1a_2X$  substrate (Figures 2B and 5C). The phenyl group at this position in **2** occupies the  $a_2$  residue binding site (W102 $\beta$ , W106 $\beta$ , and L96 $\beta$ ) and makes van der Waals contact with the lipid chain of FPP. The *N*-Boc-piperidin-4-ylmethyl moiety of **4** traverses the  $a_2$  residue-binding site and reaches into the X-residue binding site, including residues S99 $\beta$ , W102 $\beta$ , H149 $\beta$ , P152 $\beta$ , A129 $\alpha$ , Y131 $\alpha$ , and N167 $\alpha$  (Figures 2B and 5B). Two specific polar contacts are made between the Boc oxygen atoms and residues in the pocket, one each with S99 $\beta$  and W102 $\beta$ .

### Binary Complex with **5**

Although FPP was included with **5** during introduction of the inhibitor into FTase crystals (see Experimental Procedures), the inhibitor binds alone in the active site and occupies both the FPP binding pocket and the  $Ca_1a_2X$  binding pocket. Competitive binding of **5** with respect to isoprenoid was tested using steady-state kinetics measurements. Double reciprocal plots exhibited the pattern expected for competitive binding with an increase in isoprenoid  $K_m$  value in the presence of **5** without change in  $k_{cat}$  (Figure 4D).

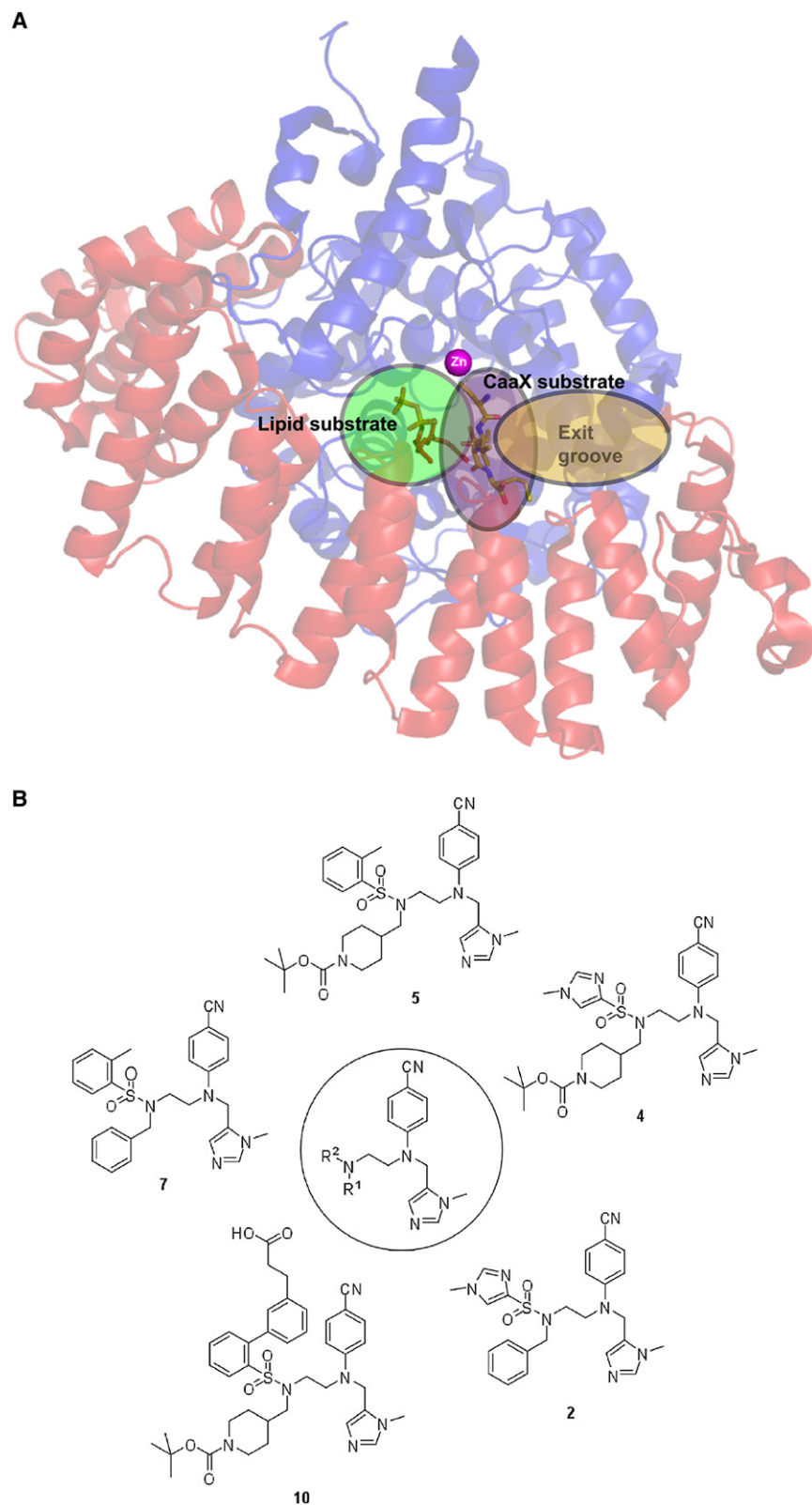


Figure 4 depicts the binding mode of **5** in the active site compared with natural substrates. Although **5** is slightly displaced toward the isoprenoid site, the *para*-benzonitrile group remains

### Figure 1. Structural Overview of FTase and Inhibitors in the Current Study

(A) Adjacent binding sites for the lipid substrate,  $\text{Ca}_1\text{a}_2\text{X}$  substrate, and displaced product in the active site of the enzyme. The  $\alpha$  subunit is shown in red, the  $\beta$  subunit is shown in blue, and the catalytic  $\text{Zn}^{2+}$  ion is shown in pink.

(B) Chemical structures of the ethylenediamine-scaffold inhibitors used in the present study.

oriented toward the exit groove, and an *N*-methylimidazole substituent coordinates the  $\text{Zn}^{2+}$ . The *o*-methylphenyl sulfonamide binds in the same place as the second isoprene of FPP, within van der Waals contact of G250 $\beta$  and Y251 $\beta$ , and one of the oxygens of the sulfonamide makes a water-mediated hydrogen bond to Y300 $\beta$ . The *N*-Boc-piperidin-4-ylmethyl binds in place of isoprene 3 of FPP, contacting residues Y205 $\beta$ , Y154 $\beta$ , W303 $\beta$ , C254 $\beta$ , and W102 $\beta$ . Water-mediated hydrogen bonds are formed between the carbonyl oxygen of the Boc group and R202 $\beta$ , and also between the piperidine nitrogen and the indole nitrogen of W106 $\beta$ .

### Derivatives of **5** Designed to Explore Bisubstrate Binding Mode

The unexpected binding mode of **5** prompted an investigation of the determinants of bisubstrate binding with several derivatives where the *o*-methylphenyl sulfonamide position was altered with additional hydrophobic and aliphatic moieties designed to further mimic parts of the isoprenoid molecule. To this end, we were successful in obtaining crystal structures of **7** and **10** bound to FTase. The biphenyl functionality in **10** was designed to mimic the lipid chain of FPP and the attached carboxylic acid group was intended to interact with the diphosphate binding pocket. Compound **7** was used to investigate whether both the *N*-Boc-piperidin-4-ylmethyl and the *o*-methylphenyl sulfonamide substituents at  $\text{R}^1$  and  $\text{R}^2$ , respectively (in **5**), were required to direct the bisubstrate binding mode, or if the *o*-methylphenyl sulfonamide alone was sufficient. As described above, **7** is a monosubstrate inhibitor (Figure 2D), suggesting the unique combination of the *o*-methylphenyl sulfonamide and the *N*-Boc-piperidin-4-ylmethyl moiety is required to direct bisubstrate binding.

The designed isoprenoid mimic **10** reverts to a monosubstrate binding mode and blocks the  $\text{Ca}_1\text{a}_2\text{X}$  binding site. Although **10**

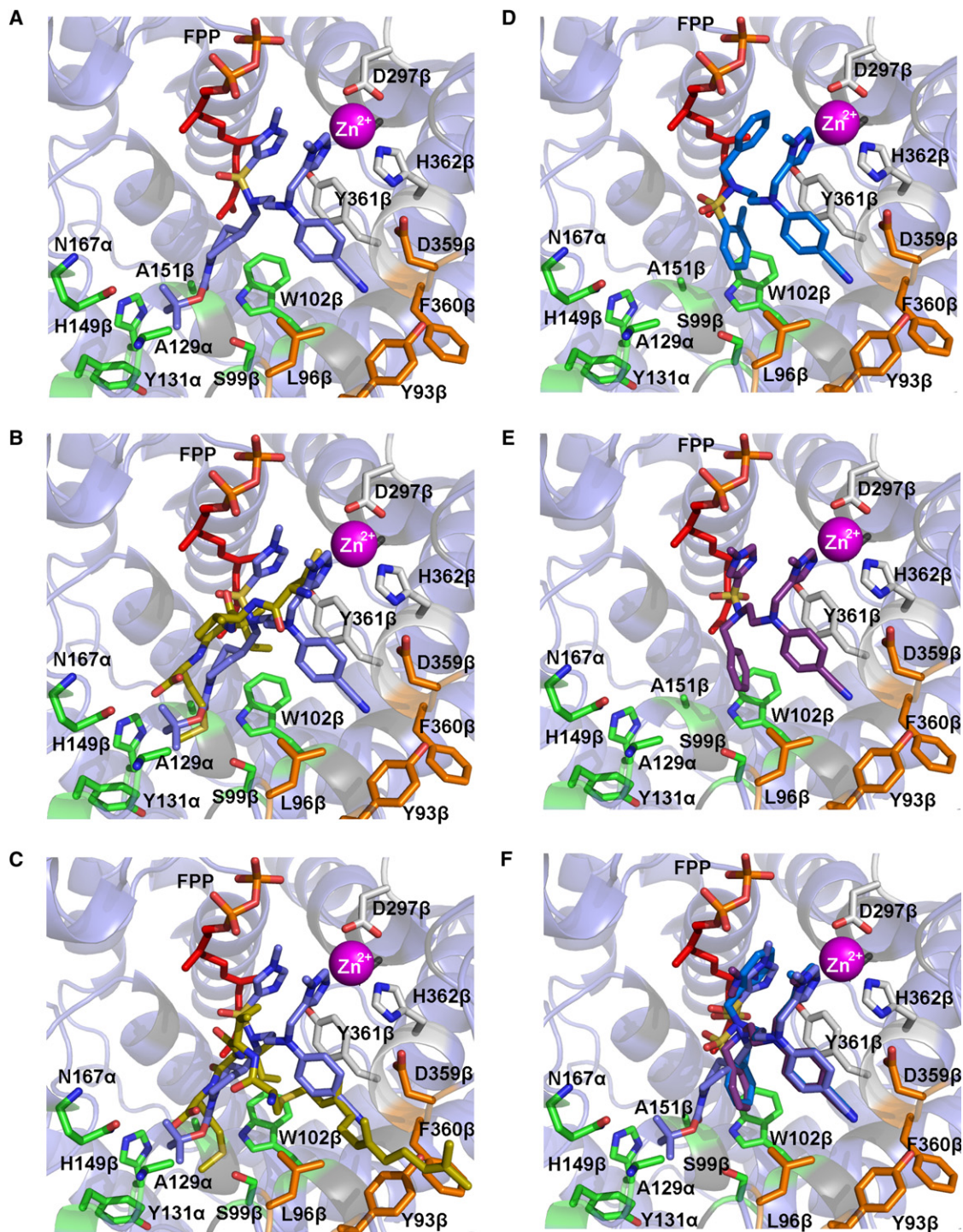


**Figure 2. Analysis of Monosubstrate Inhibitor Binding Mode**

(A) **4** (blue) bound with FPP (red) in FTase active site.

(B) Superposition of **4**:FPP structure with a  $\text{Ca}_{1,2}\text{X}$  peptide CVIM (tan) shows the monosubstrate inhibitors traverse the  $\text{Ca}_{1,2}\text{X}$  substrate binding site. The *N*-Boc-piperidin-4-ylmethyl substituent of **4** is able to reach the X-residue binding pocket (residues in green).

(C) Superposition of **4**:FPP ternary structure with a displaced CVIM product complex (tan) in the exit groove (residues in orange) illustrates contact between the inhibitor and exit groove.

(D) Binding mode of **7**.

(E) Binding mode of **2**.

(F) Superposition of monosubstrate compounds **7**, **2**, and **4** illustrate similarities in binding mode.

In all panels, the catalytic  $\text{Zn}^{2+}$  ion is shown in pink and the FTase protein is shown in gray.

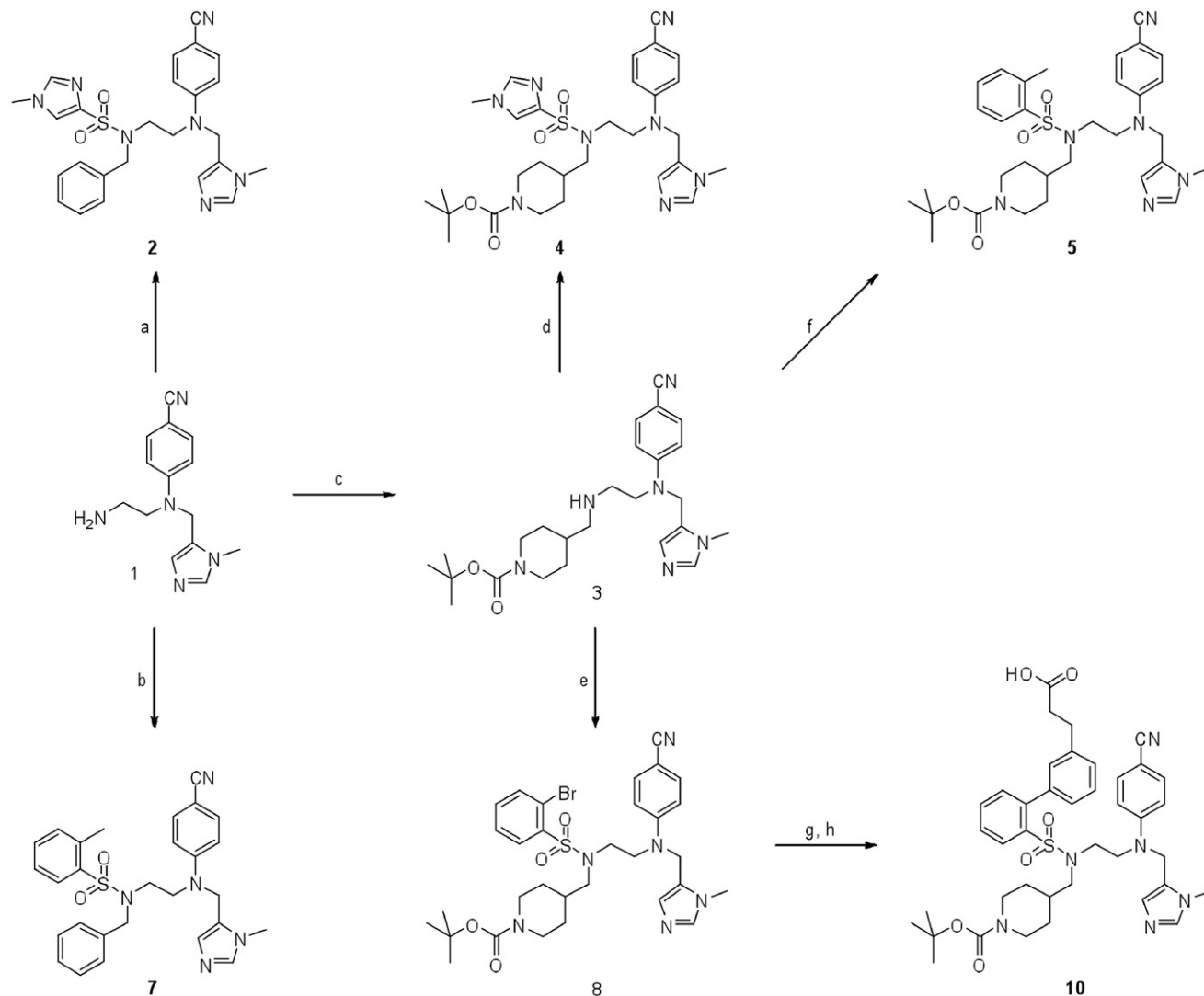


**Figure 3. Synthesis of Ethylenediamine-Scaffold Compounds in the Present Study**

- (a) 1. 1-Methyl-1*H*-imidazole-4-sulfonyl chloride, DIPEA, CH<sub>3</sub>CN, 1 hr, 0°C → rt, 93%. 2. BnBr, Cs<sub>2</sub>CO<sub>3</sub>, DMF, 16 hr, rt, 88%.  
 (b) 1. 2-Methylbenzenesulfonyl chloride, DIPEA, CH<sub>3</sub>CN, 1 hr, 0°C → rt, 92%. 2. BnBr, Cs<sub>2</sub>CO<sub>3</sub>, DMF, 16 hr, rt, 87%.  
 (c) 1. *N*-Boc-piperidin-4-ylmethylaldehyde, AcOH, 4 Å molecular sieves, MeOH, 3 hr, rt; 2. NaCNBH<sub>3</sub>, 16 hr, rt, 78%.  
 (d) 1-Methyl-1*H*-imidazole-4-sulfonyl chloride, DIPEA, CH<sub>3</sub>CN, 16 hr, 0°C → rt, 91%.  
 (e) 2-Bromobenzenesulfonyl chloride, DIPEA, CH<sub>3</sub>CN, 16 hr, 0°C → rt, 93%.  
 (f) 2-Methylbenzenesulfonyl chloride, DIPEA, CH<sub>3</sub>CN, 16 hr, 0°C → rt, 95%.  
 (g) 3-(2-Methoxycarbonyl)ethyl)phenylboronic acid, PdCl<sub>2</sub>(dppf)<sub>2</sub>, K<sub>2</sub>CO<sub>3</sub>, DMF, 16 hr, 110°C, 61%.  
 (h) LiOH·H<sub>2</sub>O, THF/MeOH/H<sub>2</sub>O, 3:1:1, 1 hr, rt, 92%.

did not bind in the designed fashion (Figure 4C), it retained potency (Table 1) against the mammalian enzyme. The positions of the Zn<sup>2+</sup> coordinating moiety and *para*-benzonitrile in the exit groove are unchanged, underscoring the role of these substituents as a dominant pharmacophore in this series. Like **7**, the sulfonamide position of **10** is directed toward the a<sub>2</sub> binding site, with the first phenyl group stabilized similarly to **7** (Figure 4C). The second phenyl group stacks on W102β, while the acid group can form polar contacts with several residues: R202β, N167α, and a water-mediated hydrogen bond with H149β. The *N*-Boc-piperidin-4-ylmethyl R<sup>1</sup> substituent of **10** extends toward the solvent making no specific polar interactions, similar to the a<sub>1</sub>

residue of the Ca<sub>1</sub>a<sub>2</sub>X substrate. This substituent is within van der Waals distance to both the first isoprene of FPP, as well as K164α, though in neither case does the interaction appear to contribute significantly to binding.

Selectivity data for **7** and **10** (Table 1) support a model in which inhibitor interactions in the divergent Ca<sub>1</sub>a<sub>2</sub>X X-residue binding pocket modulate selectivity. Like **2**, which differs only at the solvent-exposed sulfonamide position, **7** exhibits only moderate selectivity for the *P. falciparum* enzyme. **10** is significantly less selective for the *P. falciparum* enzyme than either **4** or **5**, despite full exploration of the Ca<sub>1</sub>a<sub>2</sub>X X-residue binding site. This diminished selectivity must therefore reflect the chemical nature of the

**Table 1. IC<sub>50</sub> Values and Compound Selectivity**

<i>P. falciparum</i> -selective inhibitors			
Compound	Human FTase IC <sub>50</sub> <sup>a</sup> , nM	<i>P. falciparum</i> FTase IC <sub>50</sub> <sup>b</sup> , nM	Selectivity <sup>c</sup>
<b>2</b>	56 ± 29	0.5	112
<b>4</b>	3700 ± 790	1.2	3083
<b>5</b>	4050 (n = 2)	3.0 <sup>d</sup>	1350
Probes of bisubstrate binding			
<b>7</b>	160 ± 81	5.0 <sup>e</sup>	32
<b>10</b>	800 ± 95	70.0 <sup>e</sup>	11

<sup>a</sup> Determined as described in reference (Carrico et al., 2004).

<sup>b</sup> Value from reference (Glenn et al., 2006).

<sup>c</sup> Value calculated by dividing the IC<sub>50</sub> for hFTase by the IC<sub>50</sub> for PfFTase.

<sup>d</sup> Value estimated from following values: 76% inhibition at 5 nM; 20% inhibition at 0.5 nM.

<sup>e</sup> n = 2. Determined as described in (Glenn et al., 2006).

substituent that probes this pocket (a carboxylate instead of the *N*-Boc-piperidin-4-ylmethyl group).

## DISCUSSION

The conformational flexibility, potential for introducing chemical diversity, and the favorable bioavailability properties of the ethylenediamine-scaffold inhibitors (Glenn et al., 2006) engender this series with significant potential for optimization as cancer or parasitic disease therapeutics. A summary of the structure-activity relationships determined by screening and structural studies is presented in Figure 5B. Zn<sup>2+</sup> coordination by R<sup>4</sup> is indispensable, and two substituents (R<sup>1</sup> and R<sup>3</sup>) are largely responsible for conferring selectivity profiles for mammalian and *P. falciparum* FTases. The fourth substituent (R<sup>2</sup>) does not dramatically affect selectivity, but it is critical for directing bisubstrate binding in **5**.

The switch from monosubstrate to bisubstrate binding modes as a consequence of small changes in substituent groups within a single series of FTIs is rarely observed. In the case of the dual FTase and GGTase-I inhibitor, L-778,123 (Reid et al., 2004a), small structural differences between the enzymes account for a switch in inhibition mode: in FTase L-778,123 binds only in the peptide substrate site, whereas in GGTase-I it blocks both substrates. In the L-778,123 study, subtle differences in the active sites of FTase and GGTase-I combined with additional sulfate (or phosphate) ions are sufficient to change the binding mode of L-778,123. We observe similar effects in the ethylenediamine-scaffold series. Relatively subtle differences in the structure of the inhibitor are sufficient to redirect the binding mode from monosubstrate to bisubstrate, and produce dramatically different selectivity profiles.

In the absence of a crystal structure of *P. falciparum* FTase, only a homology model can be used to identify structurally divergent regions in the active sites that potentially can be exploited to confer inhibitor selectivity. Homology models constructed by two different sequence alignment schemes predict that both the product exit groove and the pocket that binds the X-residue of the Ca<sub>1</sub>a<sub>2</sub>X motif diverge across species (Figures 5A and 5C, blue surfaces). Other major differences between the species

arise from amino acid insertions/deletions between helices in either subunit and as point mutations remote from the active site (Figure 5A, red surfaces). Although these loops are unlikely to affect catalysis directly, in aggregate these differences may alter the protein backbone sufficiently to impact binding of inhibitors at the active site. A recently described crystal structure of a non-mammalian protein prenyltransferase, the GGTase-I from the human fungal pathogen *Candida albicans*, demonstrates that sequence divergence in the exit groove contributes to significant structural changes to the protein backbone of this region (Hast and Beese, 2008).

Homology modeling of the *P. falciparum* FTase β subunit is complicated by its size (twice the length of mammalian FTase) and regions of high divergence. The first 300 amino acids exhibit no homology to either mammalian FTase or any other protein in a BLAST search, except FTases of related species of *Plasmodium*. Consequently, several different alignments can be constructed in the region of first three helices of the β subunit, where the product exit groove is predicted to be located. One alignment suggests an insertion of ~20 amino acids between helices 2 and 3 in the β subunit, thereby completely remodeling the exit groove. Even alignments that lack this insertion reveal that the exit groove is divergent.

All inhibitors presented here contact the product exit groove with a *para*-benzoxonitrile moiety. Residues that form part of the product exit groove in mammalian FTase lie in a 13-residue loop between helices 2β and 3β. The equivalent loop in *P. falciparum* FTase is predicted to share little homology with mammalian FTase (Figures 5A and 5C). Biphenyl moieties in place of the *para*-benzoxonitrile were poorly tolerated in mammalian FTase, although such derivatives retained potency against the *P. falciparum* enzyme (Glenn et al., 2006). Inspection of the crystal structures suggests that an additional phenyl ring would clash with Y93β in the exit groove (Figures 2 and 5C). As described above, the exit groove is predicted to diverge from mammalian FTase significantly; therefore, the tolerance of *P. falciparum* FTase to bulkier substituents at this position suggests that the highly diverged exit groove in this enzyme is more open, providing greater opportunities for designing selective inhibitors.

Crystal structures of FTase bound to tetrahydroquinoline (THQ)-based FTIs reveal that these compounds adopt a binding mode similar to the monosubstrate ethylenediamine-scaffold inhibitors (Eastman et al., 2007; Van Voorhis et al., 2007). Inhibitors based on either scaffold share the *N*-methylimidazole that coordinates the Zn<sup>2+</sup>, and have additional moieties that bind in the product exit groove. The crystal structure of the THQ-based FTI PB-93 bound to rat FTase reveals that an *N*-methoxycarbonyl-piperidiny-4-ylmethyl substituent binds in the pocket that binds the X-residue of the Ca<sub>1</sub>a<sub>2</sub>X motif, similar to the *N*-Boc-piperidin-4-ylmethyl of **4**. Both compounds are selective for *P. falciparum* FTase, highlighting the importance of the X-residue binding pocket and the exit groove in conferring compound selectivity (Van Voorhis et al., 2007).

Two mutations in *P. falciparum* FTase that confer resistance to THQ-based FTIs have been observed (Eastman et al., 2005; Eastman et al., 2007). Modeling the G612βA mutation (which corresponds to G250β in mammalian FTase) suggests a mechanism by which the mutation disrupts inhibitor binding by narrowing

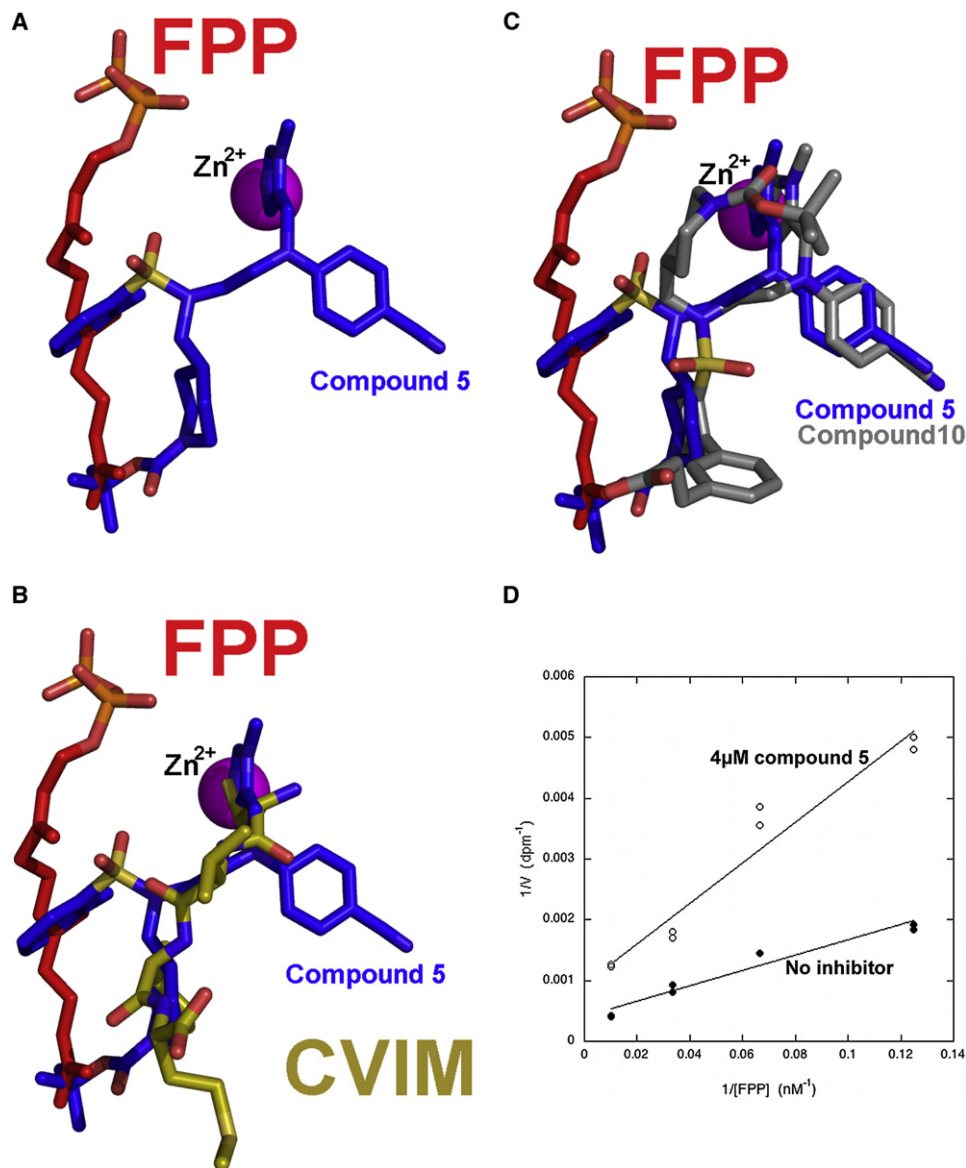


**Figure 4. Analysis of Bisubstrate Inhibitor Binding Mode**

(A) Superposition of **5** (blue) and FPP (red; from PDB 1JCR) illustrates binding of two moieties ( $R^1$  and  $R^2$ ) of the inhibitor in the isoprenoid binding site.

(B) Superposition of **5** with FPP (red; from PDB 1JCR) and CVIM  $\text{Ca}_1\text{a}_2\text{X}$  peptide (brown; from PDB 1D8D) illustrates the bisubstrate binding mode.

(C) Superposition of **5** (blue) with **10** (gray). **10** was designed to further explore bisubstrate binding by mimicking the lipid chain of FPP and phosphate moiety with a biphenyl substituent and carboxylic acid moiety. **10** clearly shifts back to monosubstrate binding; however, it does retain sub-micromolar  $\text{IC}_{50}$ .

(D) Double reciprocal plot illustrating mode of inhibition of **5**. Filled circles represent titration of FPP with no inhibitor; open circles represent the identical experiment where **5** is present at  $4 \mu\text{M}$ . Two independent experiments were performed at each FPP concentration point. Lines intersect near the y-intercept, suggesting a change in apparent  $K_m$  for FPP and therefore an isoprenoid-competitive binding mode.  $1/V$  is given in disintegrations per minute ( $\text{dpm}^{-1}$ ) for radiolabeled product using assay described in (Glenn et al., 2006).

the binding site (Eastman et al., 2007). The fused ring THQ scaffold is rigid and readily disrupted by mutations. It is tempting to speculate that the flexible nature of the ethylenediamine scaffold may be more tolerant of perturbations arising from mutations. These compounds have not yet been tested for activity against the THQ-resistant *P. falciparum* FTase mutants.

The unexpected diversity in structural binding modes observed in this study provides opportunities for exploring struc-

tural differences between target FTase enzymes for further optimization of inhibitors that are even more selective and potent for mammalian and parasite FTases.

#### SIGNIFICANCE

**Posttranslation lipidation by protein farnesyltransferase (FTase) is required for the transforming ability of oncogenic**

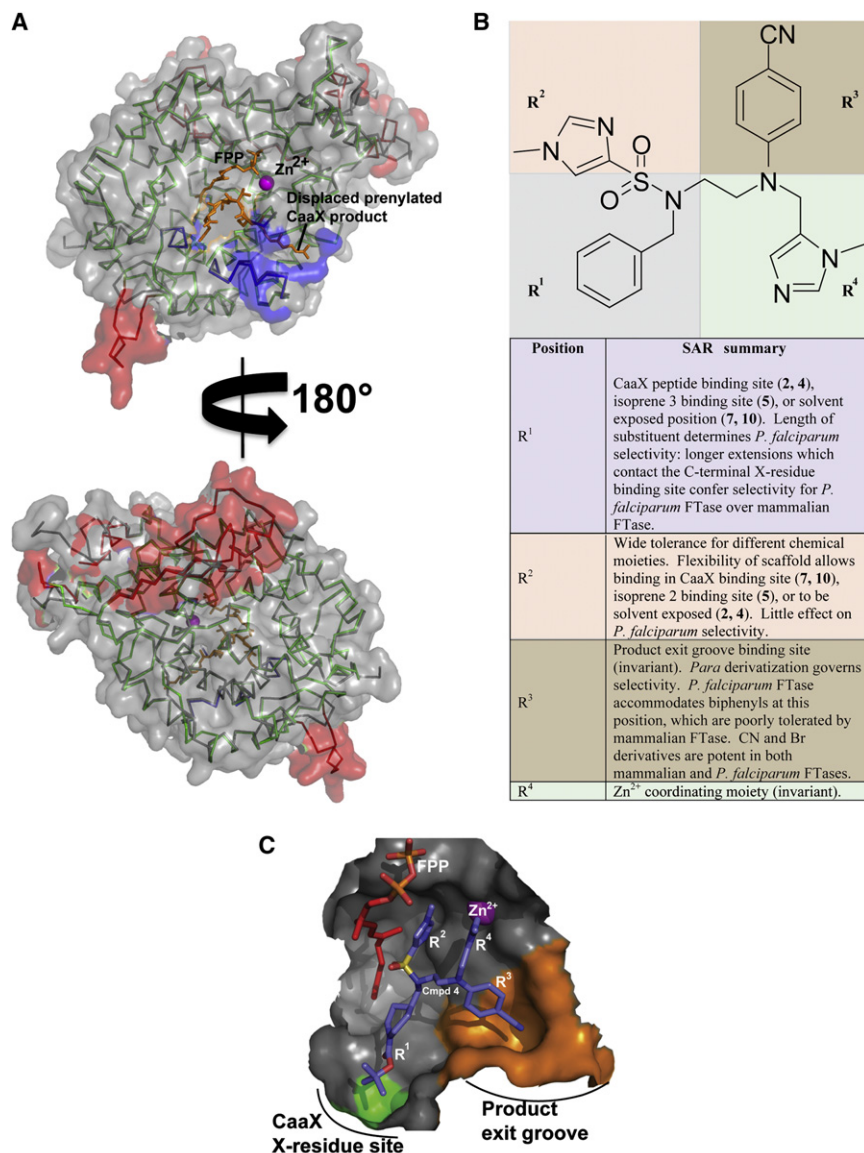


**Figure 5. Homology Modeling and Structure-Activity Summary**

(A) Homology model of the  $\beta$  subunit of *P. falciparum* FTase (gray and red ribbon) superimposed upon the  $\beta$  subunit of human FTase (green ribbon, PDB code 1TN6, chain B). The blue surfaces represent the Ca<sub>1a2</sub>X X-residue binding site and prenylated product exit groove, the two most divergent areas of the active site. The red surfaces represent the areas of  $\beta$  subunit predicted to have amino acid insertions in the *P. falciparum* enzyme not present in the mammalian enzyme.

(B) The four substituents of the ethylenediamine scaffold are correlated with the observed structure-activity relationship data as determined by screening (Glenn et al., 2006) and crystal structures.

(C) FTase active site surface with bound compound **4** and FPP. The surface is colored to represent regions of sequence diversity: orange, product exit groove; green, Ca<sub>1a2</sub>X X-residue binding site; gray, homologous residues. **4** is the most selective compound for *P. falciparum* FTase in the present study, and it contacts both regions of putative divergence in the FTase active site.

values; two have greater than 1000-fold selectivity toward *P. falciparum* FTase. Two different binding modes have been identified, including one that has interactions spanning both the peptide and farnesyl substrate-binding sites. Of particular importance to selectivity are interactions within the farnesylated peptide product “exit groove” and protein substrate binding site, the structures of which differ between species. The ethylenediamine scaffold lends itself readily to straightforward modifications that enable systematic exploration of such structural differences, which may ultimately lead to inhibitors that are sufficiently

mutants of the human Ras superfamily which are associated with 30% of all human cancers. FTase has therefore been a major focus of anticancer drug development for more than a decade. High-affinity FTase inhibitors have also emerged as a significant route for the development of new antimalarial therapeutics. Malaria currently kills over one million people each year. Furthermore, response to increasing mortality rates and emerging resistance to the current generation of antimalarials requires urgent development of new potent and selective antimalarial drugs against *Plasmodium falciparum*. Ideally such drugs exhibit high affinity for *P. falciparum* FTase and selectivity against the mammalian enzyme. The X-ray crystallographic structures of complexes of mammalian FTases with five inhibitors based on the ethylenediamine scaffold has revealed dominant structural determinants for binding and selectivity. Three of these inhibitors exhibit nanomolar IC<sub>50</sub>

inexpensive to synthesize for effective antimalarials to be economically feasible.

## EXPERIMENTAL PROCEDURES

### Chemistry, General Methods

Compounds **2** and **4** were resynthesized as described previously (Glenn et al., 2005, 2006). Synthetic procedures and characterization data for all new compounds (**5**, **7**, and **10**) are given in full below and are summarized in Figure 3. Generally, starting from **1**, inhibitors were accessed either by reaction with the appropriate sulfonyl chloride, followed by alkylation of the sulfonamide NH, or by reductive amination with *N*-Boc-piperidin-4-ylformaldehyde, followed by reaction with the appropriate sulfonyl chloride (Figure 3). Solvents CH<sub>2</sub>Cl<sub>2</sub>, CH<sub>3</sub>CN and DMF were dried on an Innovative Technology SPS-400 dry solvent system. Anhydrous MeOH and was purchased from Sigma-Aldrich and used directly from its Sure-Seal bottle. Molecular sieves were activated by heating to 300°C under vacuum overnight. All reactions were performed under an atmosphere of dry nitrogen in oven-dried glassware and were monitored for completeness by thin-layer chromatography (TLC) using silica gel (visualized

by UV light, or developed by treatment with KMnO<sub>4</sub> stain or Hanessian's stain). <sup>1</sup>H and <sup>13</sup>C NMR spectra were recorded on Bruker AM 400 MHz and Bruker AM 500 MHz spectrometers in either CDCl<sub>3</sub> or *d*<sub>4</sub>-MeOH. Chemical shifts (δ) are reported in parts per million after calibrations to residual isotopic solvent. Coupling constants (*J*) are reported in Hertz. Mass spectrometry (MS) was performed using electrospray ionization on either a Varian MAT-CH-5 (HRMS) or Waters Micromass ZQ (LRMS). Before biological testing and crystallization experiments, target molecules were subjected to further purification by reversed-phase high-performance liquid chromatography (rpHPLC). Analysis and purification by rpHPLC were performed using either Phenomenex Luna 5 μm C18 (2) 250 × 21 mm column run at 15 mL/min (preparative) or a Microsorb-MV 300 A C18 250 mm × 4.6 mm column run at 1 mL/min (analytical), using gradient mixtures of (A) water with 0.1% TFA and (B) 10:1 acetonitrile/water with 0.1% TFA. Appropriate product fractions were pooled and lyophilized to dryness, affording the inhibitors as fluffy white powders as their TFA salts. Inhibitor purity was confirmed by analytical rpHPLC using linear gradients from 100% A to 100% B, with changing solvent composition of either (I) 4.5% or (II) 1.5% per minute after an initial 2 min of 100% A. For reporting HPLC data, percentage purity is given in parentheses after the retention time for each condition.

#### 4-[(2-Aminoethyl)-(3-methyl-3H-imidazol-4-ylmethyl)-amino]-benzonitrile (1)

To a solution of 4-[(2-aminoethyl)-(3-methyl-3H-imidazol-4-ylmethyl)-amino]-benzonitrile (compound **9c** in Glenn et al., 2006) (8.0 g, 30.6 mmol) in CH<sub>2</sub>Cl<sub>2</sub> (30 ml) was added trifluoroacetic acid (30 ml). After stirring for 30 min, the reaction mixture was evaporated to dryness. The crude residue was passed through a short pad of silica (eluent: CH<sub>2</sub>Cl<sub>2</sub>/MeOH/NH<sub>4</sub>OH, 92:7:1) to furnish the title compound as the free base (7.6 g, 97%): δ<sub>H</sub> (400 MHz, CDCl<sub>3</sub>) 1.45 (br, 2H, NH<sub>2</sub>), 2.88 (t, *J* = 6.8 Hz, 2H, CH<sub>2</sub>NH<sub>2</sub>), 3.44 (t, *J* = 6.8 Hz, 2H, NH<sub>2</sub>CH<sub>2</sub>CH<sub>2</sub>), 3.55 (s, 3H, CH<sub>3</sub> (Im)), 4.55 (s, 2H, CH<sub>2</sub>Im), 6.78 (d, *J* = 8.4 Hz, 2H, 2 CH (Ar)), 6.83 (s, 1H, CH (Im)), 7.45 (s, 2H, 2 CH (Ar)), 7.47 (s, 1H, CH (Im)); δ<sub>C</sub> (125 MHz, CDCl<sub>3</sub>) 30.1, 37.0, 44.1, 49.5, 99.3, 111.7, 120.4, 127.2, 129.1, 133.0, 139.3, 150.4; HRMS (ESI) *m/z* calculated for C<sub>14</sub>H<sub>17</sub>N<sub>5</sub>H<sup>+</sup> 256.1562, found 256.1559.

#### 4-[(2-(*N*-tert-Butoxycarbonylpiperidin-4-ylmethyl)-aminoethyl)-(3-methyl-3H-imidazol-4-ylmethyl)-amino]-benzonitrile (3)

To a solution of 4-[(2-aminoethyl)-(3-methyl-3H-imidazol-4-ylmethyl)-amino]-benzonitrile (**1**; 500 mg, 1.96 mmol, 1 eq) in dry methanol (6.5 ml) was added *N*-Boc-piperidin-4-ylformaldehyde (417 mg, 1.96 mmol, 1 eq), followed by acetic acid (294 μl, 4.90 mmol, 2.5 eq) and powdered 4 Å molecular sieves (approx. 150 mg). The reaction was stirred at room temperature for 3 h, and then sodium cyanoborohydride (185 mg, 2.94 mmol, 1 eq) was added. The reaction was stirred for 18 h, then dry-loaded onto silica gel and purified by silica gel flash column chromatography (eluent: CH<sub>2</sub>Cl<sub>2</sub>/MeOH/NH<sub>4</sub>OH, 192:7:1) to provide the title compound **3** as a colorless gum (693 mg, 78%): δ<sub>H</sub> (400 MHz, CDCl<sub>3</sub>) 1.03 (m, 2H, 2 CH (piperidinylmethyl)), 1.40 (s, 9H, C(CH<sub>3</sub>)<sub>3</sub>), 1.45–1.49 (m, 1H, CH (piperidinylmethyl)), 1.58–1.61 (m, 2H, 2 CH (piperidinylmethyl)), 2.37–2.42 (m, 2H, 2 CH (piperidinylmethyl)), 2.58–2.63 (m, 2H, 2 CH (piperidinylmethyl)), 2.73 (t, *J* = 5.8 Hz, 2H, NHCH<sub>2</sub>CH<sub>2</sub>N(Im)Ar), 3.44 (m, 2H, NHCH<sub>2</sub>CH<sub>2</sub>N(Im)Ar), 3.52 (s, 3H, CH<sub>3</sub> (Im)), 4.03 (br m, 3H, NH, 2 CH (piperidinylmethyl)), 4.51 (s, 2H, CH<sub>2</sub>Im), 6.73 (s, 1H, CH (Im)), 6.76 (d, *J* = 7.6 Hz, 2H, 2 CH (Ar)), 7.39–7.41 (m, 3H, CH (Im), 2 CH (Ar)); δ<sub>C</sub> (125 MHz, CDCl<sub>3</sub>) 28.6, 30.6, 32.4, 36.8, 44.1, 45.4, 47.3, 49.5, 53.9, 79.6, 99.3, 112.9, 120.5, 127.2, 129.1, 133.7, 139.4, 151.2, 155.2; HRMS (ES+) calcd for [C<sub>25</sub>H<sub>36</sub>N<sub>6</sub>O<sub>2</sub> + H] 453.2933, found 453.2978.

#### *N*-(*N*-tert-Butoxycarbonylpiperidin-4-ylmethyl), *N*-{2-[(4-cyanophenyl)-(3-methyl-3H-imidazol-4-ylmethyl)-amino]-ethyl} 2-methylbenzenesulfonamide (5)

*N*-Boc-piperidin-4-ylmethyl bromide (61 mg, 0.221 mmol, 1.5 eq) was added to a solution of **6** (60 mg, 0.147 mmol, 1 eq) and Cs<sub>2</sub>CO<sub>3</sub> (96 mg, 0.294 mmol, 2 eq) in anhydrous DMF (1.5 ml). The reaction mixture was stirred for 48 hr at room temperature, then diluted with water (40 ml) and extracted into EtOAc (3 × 10 ml). The EtOAc extractions were combined and washed with 5% aqueous NaHCO<sub>3</sub> (3 × 10 ml), brine (10 ml), then dried (Na<sub>2</sub>SO<sub>4</sub>), filtered, and concentrated. The crude residue was purified by silica gel flash column chromatography (eluent: CH<sub>2</sub>Cl<sub>2</sub>:MeOH:NH<sub>4</sub>OH, 192:7:1) to give **5** as a colorless, waxy

solid (76 mg, 85%): δ<sub>H</sub> (400 MHz, *d*<sub>4</sub>-MeOH) 0.93 (qd, *J* = 12.1, 4.0 Hz, 2H, CH (piperidinylmethyl)), 1.48 (s, 9H, C(CH<sub>3</sub>)<sub>3</sub>), 1.51–1.60 (m, 1H, CH (piperidinylmethyl)), 1.61–1.70 (m, 2H, 2 CH (piperidinylmethyl)), 2.61 (s, 3H, CH<sub>3</sub>Ar), 2.65–2.78 (m, 2H, 2 CH (piperidinylmethyl)), 3.15 (d, *J* = 7.2 Hz, 2H, 2 CH (piperidinylmethyl)), 3.25–3.32 (m, 2H, CH<sub>2</sub>CH<sub>2</sub>NSO<sub>2</sub>), 3.56–3.62 (m, 2H, CH<sub>2</sub>CH<sub>2</sub>NSO<sub>2</sub>), 3.64 (s, 3H, CH<sub>3</sub> (Im)), 3.99–4.06 (m, 2H, 2 CH (piperidinylmethyl)), 4.65 (s, 2H, CH<sub>2</sub>Im), 6.89 (s, 1H, CH (Im)), 6.94 (d, *J* = 9.2 Hz, 2H, 2 CH (*p*-cyanoAr)), 7.40–7.46 (m, 2H, 2 CH (Ar)), 7.54 (d, *J* = 9.2 Hz, 2H, 2 CH (*p*-cyanoAr)), 7.58 (td, *J* = 7.4, 1.0 Hz, 1H, CH (Ar)), 7.71 (m, 1H, CH (Im)), 7.90 (dd, *J* = 8.0, 1.0 Hz, 1H, CH (Ar)); δ<sub>C</sub> (100 MHz, *d*<sub>4</sub>-MeOH) 20.8, 28.7, 30.8, 32.1, 36.0, 44.4 (br), 44.6, 45.3, 49.5, 55.2, 81.0, 99.8, 113.8, 121.0, 127.5, 129.0, 129.2, 130.6, 134.2, 134.3, 134.8, 139.0, 139.1, 140.5, 152.3, 156.5; HRMS (ES+) calcd for [C<sub>32</sub>H<sub>42</sub>N<sub>6</sub>O<sub>4</sub>S + H] 607.3067, found 607.3052; HPLC (I) *t*<sub>R</sub> = 13.02 min (98.7%), (II) *t*<sub>R</sub> = 20.32 min (98.6%).

#### *N*-{2-[(4-Cyanophenyl)-(3-methyl-3H-imidazol-4-ylmethyl)-amino]-ethyl} 2-methyl-benzenesulfonamide (6)

*o*-TsCl (31.2 μl, 0.216 mmol, 1.1 eq) was added dropwise to a solution of **1** (50 mg, 0.196 mmol, 1 eq) and DIPEA (68 μl, 0.392 mmol, 2 eq) in anhydrous CH<sub>3</sub>CN (2 ml). After 1 hr, TLC showed the reaction was complete. The reaction mixture was concentrated, then diluted with CH<sub>2</sub>Cl<sub>2</sub> (50 ml) and washed with water (3 × 10 ml), brine (10 ml), dried (Na<sub>2</sub>SO<sub>4</sub>), filtered, and concentrated. The residue was chromatographed on silica gel, eluting with CH<sub>2</sub>Cl<sub>2</sub>/MeOH/NH<sub>4</sub>OH, 192:7:1 to give sulfonamide **6** as a white powder (67 mg, 83%): δ<sub>H</sub> (400 MHz, *d*<sub>4</sub>-MeOH) 2.64 (s, 3H, CH<sub>3</sub>Ar), 3.15 (t, *J* = 6.4 Hz, 2H, CH<sub>2</sub>NHSO<sub>2</sub>), 3.68 (t, *J* = 6.4 Hz, 2H, CH<sub>2</sub>NHSO<sub>2</sub>), 3.93 (s, 3H, CH<sub>3</sub> (Im)), 4.82 (s, 2H, CH<sub>2</sub>Im), 6.93 (d, *J* = 9.2 Hz, 2H, 2 CH (*p*-cyanoAr)), 7.27 (s, 1H, CH (Im)), 7.37–7.43 (m, 2H, 2 CH (Ar)), 7.52–7.57 (m, 3H, 2 CH (*p*-cyanoAr), CH (Ar)), 7.91 (dd, *J* = 7.6, 1.0 Hz, 1H, CH (Ar)), 8.92 (s, 1H, CH (Im)); δ<sub>C</sub> (100 MHz, *d*<sub>4</sub>-MeOH) 20.7, 34.6, 41.2, 46.2, 51.9, 100.8, 114.4, 121.2, 127.7, 130.3, 130.4, 133.3, 8t6 134.2, 134.3, 135.2, 138.2, 138.8, 139.9, 152.1; HRMS (ES+) calcd for [C<sub>21</sub>H<sub>23</sub>N<sub>5</sub>O<sub>2</sub>S + H] 410.1651, found 410.1658.

#### *N*-Benzyl, *N*-{2-[(4-cyanophenyl)-(3-methyl-3H-imidazol-4-ylmethyl)-amino]-ethyl} 2-methyl-benzenesulfonamide (7)

Cs<sub>2</sub>CO<sub>3</sub> (96 mg, 0.294 mmol, 2 eq) was added to a solution of **3** (60 mg, 0.147 mmol, 1 eq) in anhydrous DMF (15 ml). After 10 min, benzyl bromide (19.2 μl, 0.162 mmol, 1.1 eq) was added dropwise to the reaction mixture, and then allowed to stir overnight at room temperature. The reaction mixture was diluted with water (100 ml), and the organics were extracted into EtOAc (3 × 15 ml). The EtOAc extractions were combined, washed with 5% NaHCO<sub>3</sub> solution (10 ml × 3), water (10 ml), brine (10 ml), dried (Na<sub>2</sub>SO<sub>4</sub>), filtered and concentrated. The residue was purified by silica gel flash column chromatography (eluent: CH<sub>2</sub>Cl<sub>2</sub>:MeOH:NH<sub>4</sub>OH, 192:7:1) to furnish **7** as a white foam (67 mg, 91%): δ<sub>H</sub> (500 MHz, CDCl<sub>3</sub>) 2.63 (s, 3H, CH<sub>3</sub>Ar), 3.17–3.23 (m, 2H, CH<sub>2</sub>CH<sub>2</sub>NSO<sub>2</sub>), 3.30–3.36 (m, 2H, CH<sub>2</sub>CH<sub>2</sub>NSO<sub>2</sub>), 3.45 (s, 3H, CH<sub>3</sub> (Im)), 4.29 (s, 2H, CH<sub>2</sub>Ph), 4.30 (s, 2H, CH<sub>2</sub>Im), 6.44 (d, *J* = 9.0 Hz, 2H, 2 CH (*p*-cyanoAr)), 6.69 (s, 1H, CH (Im)), 7.18–7.22 (m, 2H, 2 CH (Ar)), 7.31–7.36 (m, 7H, 5 CH (Ph), 2 CH (*p*-cyanoAr)), 7.47–7.51 (m, 2H, CH (Ar)), CH (Im)), 7.85 (dd, *J* = 7.5, 1.0 Hz, 1H, (Ar)); δ<sub>C</sub> (125 MHz, CDCl<sub>3</sub>) 20.6, 31.7, 43.7, 44.5, 48.9, 52.9, 99.3, 112.1, 119.9, 126.3, 126.7, 128.4, 128.7, 128.8, 128.9, 129.4, 133.0, 133.1, 133.6, 135.8, 137.1, 137.6, 138.9, 150.0; HRMS (ES+) calcd for [C<sub>28</sub>H<sub>29</sub>N<sub>5</sub>O<sub>2</sub>S + H] 500.2120, found 500.2121; HPLC (I) *t*<sub>R</sub> = 12.10 min (100%), *t*<sub>R</sub> = 16.78 min (100%).

#### *N*-(*N*-tert-Butoxycarbonylpiperidin-4-ylmethyl), *N*-{2-[(4-cyanophenyl)-(3-methyl-3H-imidazol-4-ylmethyl)-amino]-ethyl} 2-bromobenzenesulfonamide (8)

To an ice-cold, stirring solution of **3** (500 mg, 1.17 mmol, 1 eq) and DIPEA (310 μl, 1.78 mmol, 1.5 eq) in CH<sub>3</sub>CN (12 ml) was added 2-bromobenzenesulfonyl chloride (329 mg, 1.29 mmol, 1.1 eq). The reaction was allowed to stir for 16 hr, gradually warming to room temperature. All solvent was evaporated under reduced pressure, and the residue was then redissolved in CH<sub>2</sub>Cl<sub>2</sub> (200 ml), washed with water (30 ml), brine (30 ml), dried (Na<sub>2</sub>SO<sub>4</sub>), filtered, and concentrated. The crude material was purified by silica gel flash column chromatography (eluent: CH<sub>2</sub>Cl<sub>2</sub>:MeOH/NH<sub>4</sub>OH, 192:7:1) to afford the title compound as a white foam (731 mg, 93%): δ<sub>H</sub> (500 MHz, CDCl<sub>3</sub>) 0.90 (qd, *J* = 12.3, 4.0 Hz, 2H, 2 CH (piperidinylmethyl)), 1.33–1.39 (m, 1H, CH (piperidinylmethyl)), 1.42 (s, 9H,

**Table 2. Crystallographic Data Collection and Refinement Statistics**

	rFTase: FPP: 2 (PDB code 3E32)	rFTase: FPP: 4 (PDB code 3E30)	hFTase: 5 (PDB code 3E37)	rFTase: FPP: 7 (PDB code 3E33)	rFTase: FPP: 10 (PDB code 3E34)
Resolution range (Å)	37.5–2.45	40.7–2.45	42.8–1.80	34.0–1.90	32.2–2.05
Reflections (unique/total)	42,009/328,517	41,034/283,427	101,393/524,635	85,965/672,359	68,223/524,533
Mean I/σ <sup>a</sup>	20.2 (2.4)	22.5 (2.4)	21.9 (2.8)	34.4 (2.6)	23.2 (2.9)
R <sub>sym</sub> <sup>a</sup>	9.4 (44.9)	8.6 (33.4)	7.7 (33.5)	8.1 (55.4)	10.0 (49.5)
Completeness (%)	99.6 (95.6)	97.6 (76.8)	98.2 (93.7)	99.2 (98.0)	99.8 (98.3)
R <sub>cryst</sub> / R <sub>free</sub>	20.8/23.7	18.4/22.2	16.8/19.0	20.0/22.1	19.2/21.9
Space group: P6 <sub>1</sub>					
Unit cell dimensions: a = b (Å)	173.4	173.3	178.4	171.0	170.2
c (Å)	70.0	70.2	64.5	69.4	69.5
Rmsd from ideal geometry					
Bond lengths (Å)	0.004	0.007	0.009	0.009	0.009
Bond angles (°)	1.30	1.096	1.17	1.09	1.26
Average B factor (overall, Å <sup>2</sup> )	32	35.3	20	30	25

R<sub>sym</sub> = (Σ(|I - <I>|)/ΣI), where <I> is the average intensity of multiple measurements.

R<sub>cryst</sub> and R<sub>free</sub> = (Σ|F<sub>obs</sub> - F<sub>calc</sub>|)/(Σ|F<sub>obs</sub>|). R<sub>free</sub> was calculated over 5% of the amplitudes not used in refinement.

<sup>a</sup> Values in parentheses represent those for the highest resolution shell.

C(CH<sub>3</sub>)<sub>3</sub>, 1.49–1.56 (m, 2H, 2 CH (piperidinylmethyl)), 2.52–2.64 (m, 2H, 2 CH (piperidinylmethyl)), 3.02–3.12 (m, 2H, 2 CH (piperidinylmethyl)), 3.21–3.30 (m, 2H, CH<sub>2</sub>CH<sub>2</sub>NSO<sub>2</sub>), 3.47–3.52 (m, 2H, CH<sub>2</sub>CH<sub>2</sub>NSO<sub>2</sub>), 3.53 (s, 3H, CH<sub>3</sub> (Im)), 3.96–4.07 (m, 2H, 2 CH (piperidinylmethyl)), 4.46 (s, 2H, CH<sub>2</sub>Im), 6.72 (d, J = 9.0 Hz, 2H, 2 CH (Ar)), 6.89 (s, 1H, CH (Im)), 7.40–7.48 (m, 5H, 2 CH (Ar)), 2 CH (o-BrPh), CH (Im)), 7.73 (dd, J = 8.0, 1.5 Hz, 1H, CH (o-BrPh)), 8.08 (dd, J = 8.0, 2.0 Hz, 1H CH (o-BrPh)); δ<sub>C</sub> (125 MHz, CDCl<sub>3</sub>) 28.4, 29.5, 31.6, 34.8, 43.2 (br), 43.9, 44.3, 47.4, 54.3, 79.4, 99.8, 112.3, 119.8, 120.3, 126.5, 127.7, 129.6, 132.4, 133.8, 133.9, 135.9, 138.6, 139.3, 150.4, 154.6; HRMS (ES+) calcd for [C<sub>31</sub>H<sub>39</sub>N<sub>6</sub>O<sub>4</sub>S<sup>79</sup>Br + H] 671.2015, found 671.2029; HPLC (I) t<sub>R</sub> = 12.78 min (100%), t<sub>R</sub> = 19.92 min (100%).

***N*-(*N*-*tert*-Butoxycarbonylpiperidin-4-ylmethyl), *N*-({2-[(4-cyanophenyl)-(3-methyl-3*H*-imidazol-4-ylmethyl)-amino]-ethyl}) (3'-(2-methoxycarbonyl-ethyl)-biphenyl)-2-sulfonamide (9)**

To a round-bottomed flask was added **8** (84 mg, 0.130 mmol, 1 eq), 3-(2-methoxycarbonyl-ethyl)phenylboronic acid (41 mg, 0.196 mmol, 1.5 eq) and K<sub>2</sub>CO<sub>3</sub> (54 mg, 0.390 mmol, 3 eq). The flask was evacuated and purged with N<sub>2</sub> three times, then PdCl<sub>2</sub>(dppf)<sub>2</sub> (27 mg, 25 mol%) was added, followed by DMF (2 ml), and then the flask was evacuated and purged with N<sub>2</sub> three times again. The reaction mixture was heated to 110°C for 16 hr, then allowed to cool. Although TLC suggested only the starting aryl bromide, MS suggested the biphenyl product was present with no remaining aryl bromide, so the reaction was worked up as follows. The DMF reaction mixture was diluted with water (50 ml), then extracted into EtOAc (10 ml × 3). The EtOAc extractions were combined, then washed with water (10 ml × 3), brine (10 ml), dried (Na<sub>2</sub>SO<sub>4</sub>), filtered, and concentrated. The residue was purified by silica gel flash column chromatography (eluent: CH<sub>2</sub>Cl<sub>2</sub>/MeOH/NH<sub>4</sub>OH, 25:7:1) to give the title compound (**9**) as an off-white film (60 mg, 61%): δ<sub>H</sub> (500 MHz, CDCl<sub>3</sub>) 0.82 (qd, J = 12.3, 4.0 Hz, 2H, 2 CH (piperidinylmethyl)), 1.16–1.20 (m, 1H, CH (piperidinylmethyl)), 1.37–1.45 (m, 11H, C(CH<sub>3</sub>)<sub>3</sub>, 2 CH (piperidinylmethyl)), 2.34–2.44 (m, 2H, 2 CH (piperidinylmethyl)), 2.49–2.59 (m, 6H, CH<sub>2</sub>CH<sub>2</sub>CO<sub>2</sub>CH<sub>3</sub>, CH<sub>2</sub>CH<sub>2</sub>NSO<sub>2</sub>, 2 CH (piperidinylmethyl)), 2.89 (t, J = 7.8 Hz, 2H, CH<sub>2</sub>CH<sub>2</sub>CO<sub>2</sub>CH<sub>3</sub>), 3.24–3.31 (m, 2H, CH<sub>2</sub>CH<sub>2</sub>NSO<sub>2</sub>), 3.49 (s, 3H, CH<sub>3</sub> (Im)), 3.64 (s, 3H, CO<sub>2</sub>CH<sub>3</sub>), 3.89–4.01 (m, 2H, 2 CH (piperidinylmethyl)), 4.36 (s, 2H, CH<sub>2</sub>Im), 6.66 (d, J = 8.5 Hz, 2H, CH (p-cyanoAr)), 6.81 (s, 1H, CH (Im)), 7.10–7.13 (m, 1H, CH (Ar)), 7.16–7.27 (m, 4H, 4 CH (Ar)), 7.43 (d, J = 8.5 Hz, 2H, CH (p-cyanoAr)), 7.47 (td, J = 7.8, 1.0 Hz, 1H, CH (Ar)), 7.51 (s, 1H, Im), 7.56 (td, J = 7.8, 1.0 Hz, 1H, CH (Ar)), 8.07 (dd, J = 8.0, 1.0 Hz, 1H, CH (Ar)); δ<sub>C</sub> (125 MHz, CDCl<sub>3</sub>) 28.3, 29.4, 30.5, 31.6, 35.2, 35.3, 43.0 (br), 43.8, 44.9, 48.3, 51.6, 54.7, 79.3, 99.5, 112.2, 119.8, 126.6,

127.6, 127.7, 127.8, 127.9, 129.0, 129.9, 130.1, 132.3, 133.0, 133.7, 138.0, 139.0, 139.2, 139.9, 141.1, 150.2, 154.5, 172.9; HRMS (ES+) calcd for [C<sub>41</sub>H<sub>50</sub>N<sub>6</sub>O<sub>6</sub>S + H], 755.3591, found 755.3581; HPLC (I) t<sub>R</sub> = 13.33 min (100%), (II) t<sub>R</sub> = 21.74 min (100%).

***N*-(*N*-*tert*-Butoxycarbonylpiperidin-4-ylmethyl), *N*-({2-[(4-cyanophenyl)-(3-methyl-3*H*-imidazol-4-ylmethyl)-amino]-ethyl}) (3'-(2-carboxyethyl)-biphenyl)-2-sulfonamide (10)**

LiOH·H<sub>2</sub>O (8.7 mg, 0.207 mmol, 3 eq) was added to a solution of **9** (52 mg, 0.069 mmol, 1 eq) in a 3:1:1 mixture of THF-MeOH-H<sub>2</sub>O (1 ml). After stirring for 1 hr at room temperature, the reaction was complete. The mixture was diluted with water (50 ml), then carefully neutralized by the addition of 1N HCl. The title compound was extracted into EtOAc (10 ml × 3), dried (Na<sub>2</sub>SO<sub>4</sub>), filtered, and concentrated. The residue was chromatographed over silica gel (eluent: CH<sub>2</sub>Cl<sub>2</sub>/MeOH/NH<sub>4</sub>OH, 25:7:1) to give pure **10** as a white powder (47 mg, 92%): δ<sub>H</sub> (500 MHz, d<sub>4</sub>-MeOH) 0.86 (qd, J = 12.2, 4.0 Hz, 2H, 2 CH (piperidinylmethyl)), 1.42 (s, 9H, C(CH<sub>3</sub>)<sub>3</sub>), 1.47–1.55 (m, 3H, 3 CH (piperidinylmethyl)), 2.50 (br d, J = 7.0 Hz, 2H, 2 CH (piperidinylmethyl)), 2.57–2.67 (m, 4H, CH<sub>2</sub>CH<sub>2</sub>COOH, 2 CH (piperidinylmethyl)), 2.77–2.82 (m, 2H, CH<sub>2</sub>CH<sub>2</sub>NSO<sub>2</sub>) 2.92 (t, J = 7.5 Hz, 2H, CH<sub>2</sub>CH<sub>2</sub>COOH), 3.47–3.53 (m, 2H, CH<sub>2</sub>CH<sub>2</sub>NSO<sub>2</sub>), 3.88 (s, 3H, CH<sub>3</sub> (Im)), 3.90–3.96 (m, 2H, 2 CH (piperidinylmethyl)), 4.70 (s, 2H, CH<sub>2</sub>Im), 6.84 (d, J = 9.0 Hz, 2H, CH (p-cyanoAr)), 7.19 (s, 1H, CH (Im)), 7.21–7.32 (m, 4H, 4 CH (Ar)), 7.36 (dd, J = 7.5, 1.5 Hz, 1H, CH (Ar)), 7.54 (d, J = 9.0 Hz, 2H, CH (p-cyanoAr)), 7.61 (td, J = 7.5, 1.0 Hz, 1H, CH (Ar)), 7.69 (td, J = 7.5, 1.0 Hz, 1H, CH (Ar)), 8.16 (dd, J = 8.0, 1.0 Hz, 1H, CH (Ar)), 8.91 (s, 1H, CH (Im)); δ<sub>C</sub> (125 MHz, d<sub>4</sub>-MeOH) 28.7, 30.7, 31.7, 34.3, 36.4, 36.6, 44.3 (br), 45.3, 46.8, 50.9, 56.0, 81.1, 100.7, 114.1, 119.1, 120.8, 129.0, 129.1, 129.3, 129.4, 131.3, 131.5, 133.0, 133.9, 134.5, 134.9, 137.9, 139.5, 140.9, 142.0, 142.8, 151.5, 156.5, 176.3; HRMS (ES+) calcd for [C<sub>40</sub>H<sub>46</sub>N<sub>6</sub>O<sub>6</sub>S + H], 741.3434, found 741.3436; HPLC (I) t<sub>R</sub> = 12.99 min (100%), (II) t<sub>R</sub> = 19.68 min (100%).

**Protein Preparation and Crystallization**

Wild-type rat and human protein farnesyltransferases (rFTase and hFTase, respectively) were expressed and purified as described (Chen et al., 1993; Long et al., 2001). Crystals of rFTase containing a farnesylated KKKSCKTQVIM peptide were prepared as described (Long et al., 2002). Similarly, crystals of wild-type hFTase were prepared containing farnesylated DDPTASACVLS or DDPTASACNIQ peptides as described (Terry et al., 2006). All compounds were furnished as lyophilized solids and were solubilized in dimethyl sulfoxide to prepare a stock solution with a concentration of 30 mM. Inhibitors were

introduced into the FTase active site by soaking preformed product complex crystals in a stabilizing solution supplemented with 100  $\mu\text{M}$  FPP and 300  $\mu\text{M}$  inhibitor for 5 to 7 days, followed by cryoprotection and flash cooling in liquid nitrogen as described (Reid and Beese, 2004; Reid et al., 2004a).

#### Data Collection, Model Building, and Refinement

X-ray diffraction data were collected at the Southeast Regional Collaborative Access Team (SER-CAT) 22-BM beamline at the Advanced Photon Source, Argonne National Laboratory. Data reduction and scaling were performed with HKL2000 (Otwinowski and Minor, 1997). Phases were calculated using molecular replacement as implemented by PHASER in the CCP4 suite (Storoni et al., 2004). Iterative model building and refinement were performed using Coot and REFMAC5, respectively (Emsley and Cowtan, 2004; Murshudov et al., 1997). MOLPROBITY was used to calculate a Ramachandran plot, identify and correct rotamer outliers, and identify any potential steric clashes in the models (Davis et al., 2004). Figures illustrating the determined structures and superpositions were prepared with Pymol (Delano, 2002). Data collection and refinement statistics are contained in Table 2. The atomic coordinates have been deposited with the RCSB Protein Data Bank with the following PDB ID codes: 3E30, 3E32, 3E33, 3E34, and 3E37. Multiple homology models of *P. falciparum* FTase were prepared with web-based servers Swiss Model (Guex and Peitsch, 1997) and Phyre (Bennett-Lovsey et al., 2008) using alignments prepared by the modeling program based upon input crystal structure (PDB code 1TN6) or a user-defined alignment prepared in ClustalW (Thompson et al., 1994).

#### Activity Assays

We determined the effect of the ethylenediamine-based compounds on their abilities to inhibit human FTase activity of 60,000  $\times$  g supernatants of human Burkitt's lymphoma (Daudi) cells (American Type Culture Collection, Rockville, MD) as described (Carrico et al., 2004). Inhibition studies were performed to determine the ability of hFTase to transfer [3H]farnesyl from [3H]farnesylpyrophosphate (GE Biosciences, Piscataway, NJ) to recombinant human H-Ras. After a 30-min incubation in the presence of the inhibitor, H-Ras protein was precipitated with trichloroacetic acid, filtered onto glass fiber filters, and filters were washed thoroughly to remove unbound [3H]farnesylpyrophosphate from the filter. Activity of dried filters was counted on a scintillation counter, and activities of samples treated with compound were compared with those treated with vehicle alone to determine  $\text{IC}_{50}$  values. Results shown are the mean/standard deviation of at least three independent experiments, except for **5**, for which the value was the mean of two replicates. The  $\text{IC}_{50}$  determinations for *P. falciparum* FTase **2** and **4** listed in Table 1 were obtained from reference (Glenn et al., 2006). For **7** and **10** we calculated the  $\text{IC}_{50}$  according to the methods in (Glenn et al., 2006). For **5**, we titrated the inhibitory activity of the compound and determined the  $\text{IC}_{50}$  by interpolation from points above and below the 50% inhibition of enzyme activity (76% and 20% inhibitory activity, respectively). The activity assay used to estimate the  $\text{IC}_{50}$  of **5**, **7**, and **10** was performed as described (Glenn et al., 2006).

Assays to determine the mode of competition of **5** were conducted as described above for human FTase, except that the source of enzyme was purified hFT from *E. coli*. FPP concentration was varied at constant H-Ras substrate and inhibitor concentrations. Data were analyzed using a standard Lineweaver-Burk double reciprocal plot to visualize inhibition patterns.

#### ACKNOWLEDGMENTS

This work was supported by NIH Grants GM52382 (to L.S.B), CA067771 (to S.M.S and A.D.H.), and AI054384 (to M.H.G and W.C.V.). Use of the Advanced Photon Source was supported by the U.S. Department of Energy, Office of Science, Office of Basic Energy Sciences under Contract No. W-31-109-Eng-38. We thank Matthew Glenn and Sung-Yoon Chang for their early work on the design and synthesis of several compounds.

Received: September 1, 2008

Revised: January 21, 2009

Accepted: January 26, 2009

Published: February 26, 2009

#### REFERENCES

- Basso, A.D., Kirschmeier, P., and Bishop, W.R. (2006). Lipid posttranslational modifications. Farnesyl transferase inhibitors. *J. Lipid Res.* *47*, 15–31.
- Bell, I.M., Gallicchio, S.N., Abrams, M., Beese, L.S., Beshore, D.C., Bhimnathwala, H., Bogusky, M.J., Buser, C.A., Culbertson, J.C., Davide, J., et al. (2002). 3-Aminopyrrolidinone farnesyltransferase inhibitors: design of macrocyclic compounds with improved pharmacokinetics and excellent cell potency. *J. Med. Chem.* *45*, 2388–2409.
- Bennett-Lovsey, R.M., Herbert, A.D., Sternberg, M.J., and Kelley, L.A. (2008). Exploring the extremes of sequence/structure space with ensemble fold recognition in the program Phyre. *Proteins* *70*, 611–625.
- Carrico, D., Ohkanda, J., Kendrick, H., Yokoyama, K., Blaskovich, M.A., Bucher, C.J., Buckner, F.S., Van Voorhis, W.C., Chakrabarti, D., Croft, S.L., et al. (2004). In vitro and in vivo antimalarial activity of peptidomimetic protein farnesyltransferase inhibitors with improved membrane permeability. *Bioorg. Med. Chem.* *12*, 6517–6526.
- Casey, P.J., and Seabra, M.C. (1996a). Protein prenyltransferases. *J. Biol. Chem.* *271*, 5289–5292.
- Casey, P.J., and Seabra, M.C. (1996b). Protein prenyltransferases. *J. Biol. Chem.* *271*, 5289–5292.
- Chen, W.J., Moomaw, J.F., Overton, L., Kost, T.A., and Casey, P.J. (1993). High level expression of mammalian protein farnesyltransferase in a baculovirus system. The purified protein contains zinc. *J. Biol. Chem.* *268*, 9675–9680.
- Davis, I.W., Murray, L.W., Richardson, J.S., and Richardson, D.C. (2004). MOLPROBITY: structure validation and all-atom contact analysis for nucleic acids and their complexes. *Nucleic Acids Res.* *32*, W615–619.
- Delano, W.L. (2002). The PyMOL molecular graphics system (San Carlos, CA: DeLano Scientific).
- Dolence, J.M., Cassidy, P.B., Mathis, J.R., and Poulter, C.D. (1995). Yeast protein farnesyltransferase: steady-state kinetic studies of substrate binding. *Biochemistry* *34*, 16687–16694.
- Eastman, R.T., White, J., Hucke, O., Bauer, K., Yokoyama, K., Nallan, L., Chakrabarti, D., Verlinde, C.L., Gelb, M.H., Rathod, P.K., et al. (2005). Resistance to a protein farnesyltransferase inhibitor in *Plasmodium falciparum*. *J. Biol. Chem.* *280*, 13554–13559.
- Eastman, R.T., Buckner, F.S., Yokoyama, K., Gelb, M.H., and Van Voorhis, W.C. (2006). Thematic review series: lipid posttranslational modifications. Fighting parasitic disease by blocking protein farnesylation. *J. Lipid Res.* *47*, 233–240.
- Eastman, R.T., White, J., Hucke, O., Yokoyama, K., Verlinde, C.L., Hast, M.A., Beese, L.S., Gelb, M.H., Rathod, P.K., and Van Voorhis, W.C. (2007). Resistance mutations at the lipid substrate binding site of *Plasmodium falciparum* protein farnesyltransferase. *Mol. Biochem. Parasitol.* *152*, 66–71.
- Emsley, P., and Cowtan, K. (2004). Coot: model-building tools for molecular graphics. *Acta Crystallogr. D Biol. Crystallogr.* *60*, 2126–2132.
- Furfine, E.S., Leban, J.J., Landavazo, A., Moomaw, J.F., and Casey, P.J. (1995). Protein farnesyltransferase: Kinetics of farnesyl pyrophosphate binding and product release. *Biochemistry* *34*, 6857–6862.
- Glenn, M.P., Chang, S.Y., Hucke, O., Verlinde, C.L., Rivas, K., Horney, C., Yokoyama, K., Buckner, F.S., Pendyala, P.R., Chakrabarti, D., et al. (2005). Structurally simple farnesyltransferase inhibitors arrest the growth of malaria parasites. *Angew. Chem. Int. Ed. Engl.* *44*, 4903–4906.
- Glenn, M.P., Chang, S.Y., Horney, C., Rivas, K., Yokoyama, K., Pusateri, E.E., Fletcher, S., Cummings, C.G., Buckner, F.S., Pendyala, P.R., et al. (2006). Structurally simple, potent, *Plasmodium* selective farnesyltransferase inhibitors that arrest the growth of malaria parasites. *J. Med. Chem.* *49*, 5710–5727.
- Guex, N., and Peitsch, M.C. (1997). SWISS-MODEL and the Swiss-PdbViewer: an environment for comparative protein modeling. *Electrophoresis* *18*, 2714–2723.
- Hast, M.A., and Beese, L.S. (2008). Structure of protein geranylgeranyltransferase-I from the human pathogen *Candida albicans* complexed with a lipid substrate. *J. Biol. Chem.* *283*, 31933–31940.

- Hightower, K.E., Huang, C.-C., Casey, P.J., and Fierke, C.A. (1998). H-ras peptide and protein substrates bind protein farnesyltransferase as an ionized thiolate. *Biochemistry* 37, 15555–15562.
- Huang, C., Hightower, K.E., and Fierke, C.A. (2000). Mechanistic studies of rat protein farnesyltransferase indicate an associative transition state. *Biochemistry* 39, 2593–2602.
- Konstantinopoulos, P.A., Karamouzis, M.V., and Papavassiliou, A.G. (2007). Post-translational modifications and regulation of the RAS superfamily of GTPases as anticancer targets. *Nat. Rev. Drug Discov.* 6, 541–555.
- Lane, K.T., and Beese, L.S. (2006). Thematic review series: lipid posttranslational modifications. Structural biology of protein farnesyltransferase and geranylgeranyltransferase type I. *J. Lipid Res.* 47, 681–699.
- Long, S.B., Casey, P.J., and Beese, L.S. (1998). Cocrystal structure of protein farnesyltransferase complexed with a farnesyl diphosphate substrate. *Biochemistry* 37, 9612–9618.
- Long, S.B., Casey, P.J., and Beese, L.S. (2000). The basis for K-Ras4B binding specificity to protein farnesyltransferase revealed by 2 Å resolution ternary complex structures. *Structure* 8, 209–222.
- Long, S.B., Hancock, P.J., Kral, A.M., Hellinga, H.W., and Beese, L.S. (2001). The crystal structure of human protein farnesyltransferase reveals the basis for inhibition by CaaX tetrapeptides and their mimetics. *Proc. Natl. Acad. Sci. USA* 98, 12948–12953.
- Long, S.B., Casey, P.J., and Beese, L.S. (2002). Reaction path of protein farnesyltransferase at atomic resolution. *Nature* 419, 645–650.
- Murshudov, G.N., Vagin, A.A., and Dodson, E.J. (1997). Refinement of macromolecular structures by the maximum-likelihood method. *Acta Crystallogr. D Biol. Crystallogr.* 53, 240–255.
- Otwinowski, Z., and Minor, W. (1997). Processing of X-ray diffraction data collected in oscillation mode. *Methods Enzymol.* 276, 307–326.
- Pickett, J.S., Bowers, K.E., Hartman, H.L., Fu, H.W., Embry, A.C., Casey, P.J., and Fierke, C.A. (2003). Kinetic studies of protein farnesyltransferase mutants establish active substrate conformation. *Biochemistry* 42, 9741–9748.
- Reid, T.S., and Beese, L.S. (2004). Crystal structures of the anticancer clinical candidates R115777 (Tipifarnib) and BMS-214662 complexed with protein farnesyltransferase suggest a mechanism of FTI selectivity. *Biochemistry* 43, 6877–6884.
- Reid, T.S., Long, S.B., and Beese, L.S. (2004a). Crystallographic analysis reveals that anticancer clinical candidate L-778,123 inhibits protein farnesyltransferase and geranylgeranyltransferase-I by different binding modes. *Biochemistry* 43, 9000–9008.
- Reid, T.S., Terry, K.L., Casey, P.J., and Beese, L.S. (2004b). Crystallographic analysis of CaaX prenyltransferases complexed with substrates defines rules of protein substrate selectivity. *J. Mol. Biol.* 343, 417–433.
- Storoni, L.C., McCoy, A.J., and Read, R.J. (2004). Likelihood-enhanced fast rotation functions. *Acta Crystallogr. D Biol. Crystallogr.* 60, 432–438.
- Taylor, J.S., Reid, T.S., Terry, K.L., Casey, P.J., and Beese, L.S. (2003). Structure of mammalian protein geranylgeranyltransferase type-I. *EMBO J.* 22, 5963–5974.
- Terry, K.L., Casey, P.J., and Beese, L.S. (2006). Conversion of protein farnesyltransferase to a geranylgeranyltransferase. *Biochemistry* 45, 9746–9755.
- Thompson, J.D., Higgins, D.G., and Gibson, T.J. (1994). CLUSTAL W: improving the sensitivity of progressive multiple sequence alignment through sequence weighting, position-specific gap penalties and weight matrix choice. *Nucleic Acids Res.* 22, 4673–4680.
- Tschantz, W.R., Furfine, E.S., and Casey, P.J. (1997). Substrate binding is required for release of product from mammalian protein farnesyltransferase. *J. Biol. Chem.* 272, 9989–9993.
- Van Voorhis, W.C., Rivas, K.L., Bendale, P., Nallan, L., Horney, C., Barrett, L.K., Bauer, K.D., Smart, B.P., Ankala, S., Hucke, O., et al. (2007). Efficacy, pharmacokinetics, and metabolism of tetrahydroquinoline inhibitors of Plasmodium falciparum protein farnesyltransferase. *Antimicrob. Agents Chemother.* 51, 3659–3671.
- Zhang, F.L., and Casey, P.J. (1996). Influence of metal ions on substrate binding and catalytic activity of mammalian protein geranylgeranyltransferase type-I. *Biochem. J.* 320, 925–932.